Lateral capacity and repair of corrosion-damaged pile bents, part 1: Design and testing considerations

Gray Mullins, Rajan Sen, Andrew Goulish, and Danny Winters

- The effects of corrosion damage in prestressed piles are difficult to quantify because the amounts of steel loss are unknown.
- This paper, which is the first in a three-part series highlighting the test methodologies and effects of corrosion damage on bridge pile bents, provides the basis of comparison for two subsequent papers.
- Part 2 will address the design of carbon-fiber-reinforced polymer (CFRP) repairs for corroded piles, and part 3 will present test results for a severely corroded pile bent where full lateral capacity was restored using CFRP repairs.

A pile bent is a type of bridge pier where the piles extend from the soil-bearing stratum to the underside of the girders. A reinforced concrete beam (pile cap) ties the piles together into a structural frame and provides for beam seats, bearing pads, or both. Whereas vessel-collision forces typically control present-day overwater bridge pier designs, bridges built before the 1980s used shorter span lengths and low water-clearance heights to minimize costs. From the 1940s to the 1990s, clearance requirements progressively increased out of necessity. The initial increases were made to prevent seawater from spraying vehicles, and subsequent increases were intended to address storm surges that can dislodge deck assemblies and to control corrosion damage to the girders. Foundation components (piles, footings, or columns) will always be vulnerable to corrosion.

Piers subjected to extreme-event lateral forces can require many more piles than those required to support only self-weight and vehicular loads. Therefore, when span lengths are determined, owners and designers must evaluate the costs of using more-expensive longer, deeper girders as well as the number of pier locations with large, vessel collision–resistant footings. Without considering vessel-collision forces or knowledge of the effects of corrosion damage on service life, cost analyses in the past tended to favor shorter spans with small, low-height pile bent–type piers. **Figure 1** shows three adjacent bridges built in the 1950s, 1970s, and 1990s, which were surveyed as part of the project described in this article. The girder clearances from high water were

Figure 1. Bridge design transition from lower to higher overwater clearance. Note: 1 ft = 0.305 m.

1.8, 2.4, and 3.6 m (5.9, 7.9, and 12 ft) for the 1950s-, 1970s-, and 1990s-era structures, respectively. The 1950s- and 1970s-era bridges had pile-bent-type piers. The 1950s-era bridge was recently dismantled after severe corrosion damage of the seawater-sprayed girders led to falling debris.[1]

The number of reinforced or prestressed concrete piles making a bent is dictated by the bridge width, the number of girders (typically one pile per girder), or both the bridge width and the number of girders. Historically, battered, or raked, piles were used to withstand sidesway from wind loads and longitudinal braking forces, but battered piles were found to attract the majority of lateral loads and could fail prematurely.[2] Today, vertical prestressed piles are the norm, with all piles sharing the bending stresses from lateral loads more uniformly.

Piles in bridges spanning over coastal or tidal waters are subjected to saltwater tidal cycles that promote corrosion. Corrosion is particularly problematic in driven prestressed concrete piles in the "splash zone," which is defined by the Florida Department of Transportation (FDOT) to be a 4.9 m (16 ft) high region extending 1.2 m (3.9 ft) below the mean lower-water level and 3.7 m (12 ft) above the mean high-water level.[3] The highest levels of chloride contamination occur in the 1.68 m (5.51 ft) region of the pile directly above the high-water level, where chloride contamination results from wetting-and-drying cycles, and from salt deposition from seawater spray. In this region of the pile, the surface chloride concentration is much higher than the concentration in seawater itself, and the high amount of chloride on the surface in turn accelerates chloride diffusion through the typical 76 mm (3.0 in.) thick required cover. In extremely aggressive environments, substructure elements such as footings and columns require 102 mm (4.0 in.) cover and drilled shafts require 152 mm (6.0 in.) cover.[3,4]

Despite the trend away from pile bent–type piers in current designs, structures with bent-type piers still comprise a large fraction of the coastal bridge inventory, and many of those structures are reaching or have passed their anticipated service lives. In Florida, 43% of the 12,595 bridges in the FDOT inventory were built in the 1950s, 1960s, or 1970s, a time when pile bents were used almost exclusively for shorter piers because they were economical and because vessel collisions were not commonly considered in the design process.[5] **Figure 2** shows a typical 1960s-era bridge in service today in south Florida; its shorter piers are pile bents, and the taller piers are cap-and-column-type designs.

Pile bents are essentially portal frames, where exposed longer pile lengths create higher pile-bending moments near the cap from lateral loads. For bridges where the splash zone and highest bending moment regions coincide, the probability of corrosion damage adversely affecting performance is increased. **Figure 3** shows two bridges where the splash-zone damage location varies relative to the underside of the pile cap where bending moments are highest.

Figure 2. Pile cap and column– and pile bent–type piers (built 1969).

Figure 3. Corrosion damage near pile cap (left) and corrosion damage farther from high bending moment region (right).

A review of site surveys of 74 pile bent–type piers from 14 FDOT bridges with splash-zone corrosion damage concluded that most pile bents had four to six piles, pile sizes ranged from 0.3 to 0.61 m (12 to 24 in.), and the most common pile size was 0.46 m (1.5 ft).[6–8] The slenderness ratio L/r ranged from 48.5 to 99.1 (average 63), where L was the length of pile from the underside of the cap to the point of fixity below ground and the radius of gyration r was taken to be $0.3D$ (where D is pile diameter). On average, the location of damage from the underside of the cap was found to be $0.2L$. Therefore, for the average pile size of 0.46 m, the corresponding L would be $63 \times 0.3D$, or 8.6 m (28 ft), and the average location to the center of corrosion damage would be 1.74 m (5.71 ft) from the underside of pile cap. Given that the highest chloride contamination region is 1.68 m (5.51 ft) long, the center of damage would be 0.83 m (2.7 ft) above high water and the average pile cap bottom would be 2.6 m (8.5 ft) above sea level. The mudline was 6.8 m (22 ft) from the bottom of pile cap on average, so the average water depth would be approximately 4.2 m (14 ft) (**Fig. 4**). This information was vital in creating a test setup to represent the effects of corrosion damage on lateral pile bent capacity.

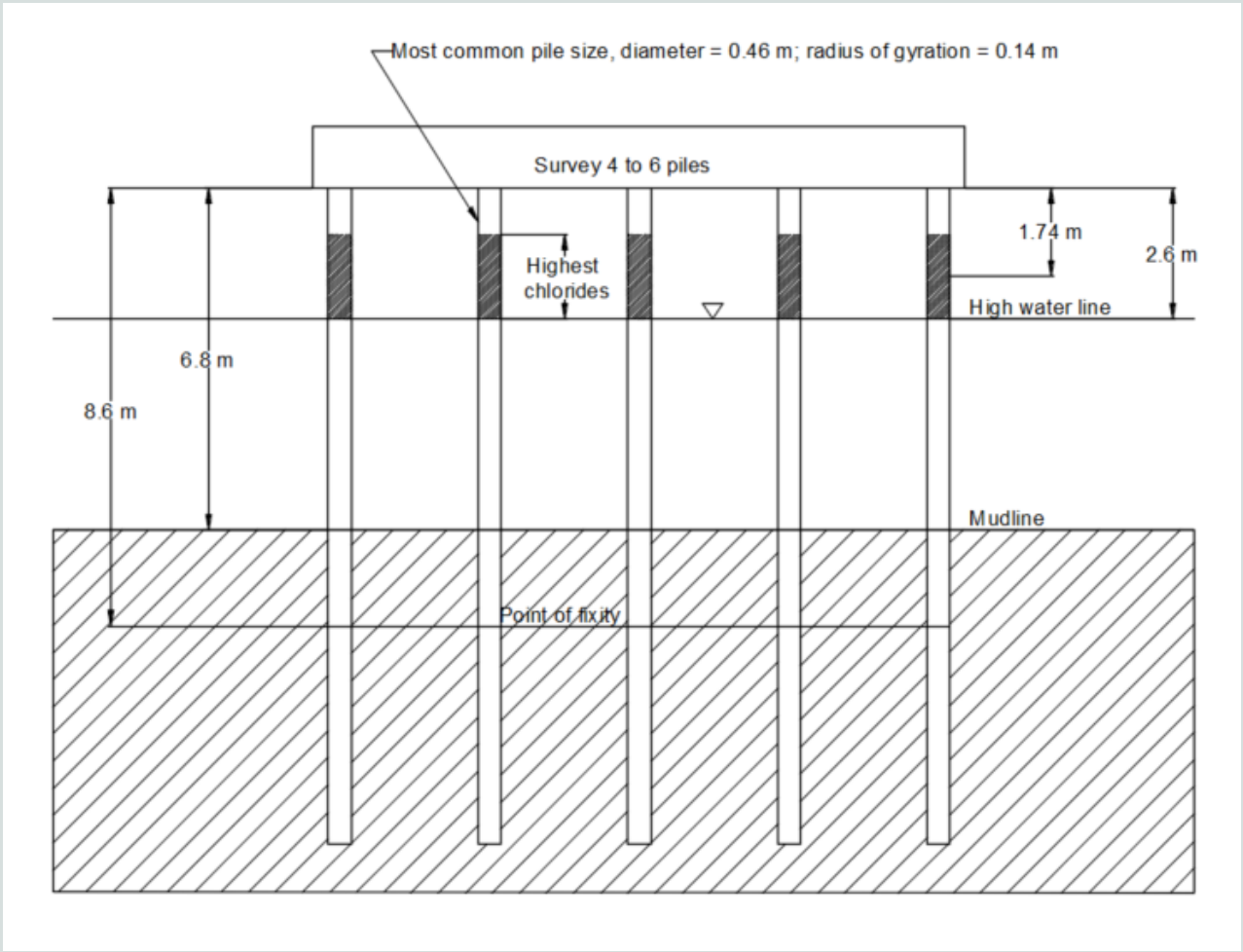

Figure 4. Summary or bridge survey showing most common dimensions. Note: 1 m = 3.281 ft.

This paper is the culmination of a 25-year study to assess the loss in lateral capacity of pile bents from corrosion damage, the design and modeling of a viable strength-restoration alternative, and verification testing of a repaired pile bent after 20 years of outdoor exposure.

Objectives and scope

The objectives of the study were to simulate corrosion damage found in field piles, identify the magnitude of lateral capacity loss as piles in a simulated bridge bent undergo progressive corrosion damage to an area up a 50% steel loss, develop a viable repair scheme, and repair and retest the same simulated bridge configuration when 100% of the steel cross section is lost.

The initial scope of the project was to demonstrate lateral capacity loss as a function of corroded strand area loss; however, subsequent advancements in fiber-reinforced polymer (FRP) repair technology for underwater applications[9,10] led the investigators to expand the project scope to include further testing. The additional efforts involved numerical modeling and design of a suitable FRP repair to fully restore the original pile bent capacity. Piles corroded to 50% steel loss were set aside in an outdoor storage compound in 2000, retrieved in 2020, repaired with carbon FRPs (CFRPs) and used in the reconstruction of a pile bent identical to those tested in 2000 and 2001. Because each phase of the study was critically important, the findings of the research are presented in three parts as follows:

- Part 1 covers testing of corroded pile bridge bents.
- Part 2 covers the design and numerical modeling of FRP repairs for corrosion-damaged bridge bents.
- Part 3 covers CFRP repair and strength restoration of a corrosion-damaged pile bent.

This paper (part 1) covers the development of the bridge bent test setup, an accelerated corrosion procedure to induce a predictable level of corrosion damage in subject piles, and lateral-load testing of simulated bridge bents. This test configuration forms the comparative basis for the subsequent papers that will address FRP repair and capacity verification of a repaired pile bent.

Approach

The development of a testing methodology revolved around replicating the bending moment distribution in a pile bent when the bent was exposed to lateral loading. Pile caps that provide complete fixity create the highest bending moments in the piles immediately below the cap. In contrast, a pinned connection to a pile cap produces the highest bending moments well below the mudline at the point of fixity, the depth of which is dependent on the lateral soil modulus and the associated stiffness. For this study, it was necessary to determine a suitable pile cap fixity and requirements for soil embedment simulation in laboratory conditions.

The use of rigid pile-to-cap connections is not usually needed for at-grade footings; however, it can reduce the worst-case internal pile-bending moment, which then reduces the size and cost of the overall foundation system. This is especially true in overwater bridge piers with exposed, long pile lengths between the cap and mudline. Castilla et al.[11] presented the bending moment diagram for an HP14x117 steel bearing pile embedded 1.2 and 0.3 m (3.9 and 1 ft) into the pile cap along with an idealized no-embedment condition (**Fig. 5**).[11] With loss of pile-to-cap fixity (reduced embedment), the moment in the pile at the base of the cap decreases and the maximum moment increases and moves into the soil embedment region. These model results also show no moment in the pile inside the cap at an embedment of approximately 0.9 m (3 ft), suggesting that for this case (cited to be a 67 kN [15 kip] lateral load, 360 mm [14 in.] pile size, and 35.12 MPa [5094 psi] concrete cap strength), 0.9 m is the minimum required pile-in-cap embedment depth. However, the pile section has a yielding bending capacity that is eight times higher (969 kN-m [8580 kip-in.]) than that developed by the cited loading, so it is unclear whether the full bending capacity of the pile could be developed based on this data, or whether additional embedment length would be required to provide complete fixity.

Figure 5 also shows a concept moment diagram presented by Joen and Park[12] that incorrectly shows the magnitude of moment to be higher below ground when the cap is supposedly fixed. This diagram was most likely intended to show the general shape of the moment and was not intended to be interpreted as being to scale. This diagram has led to much

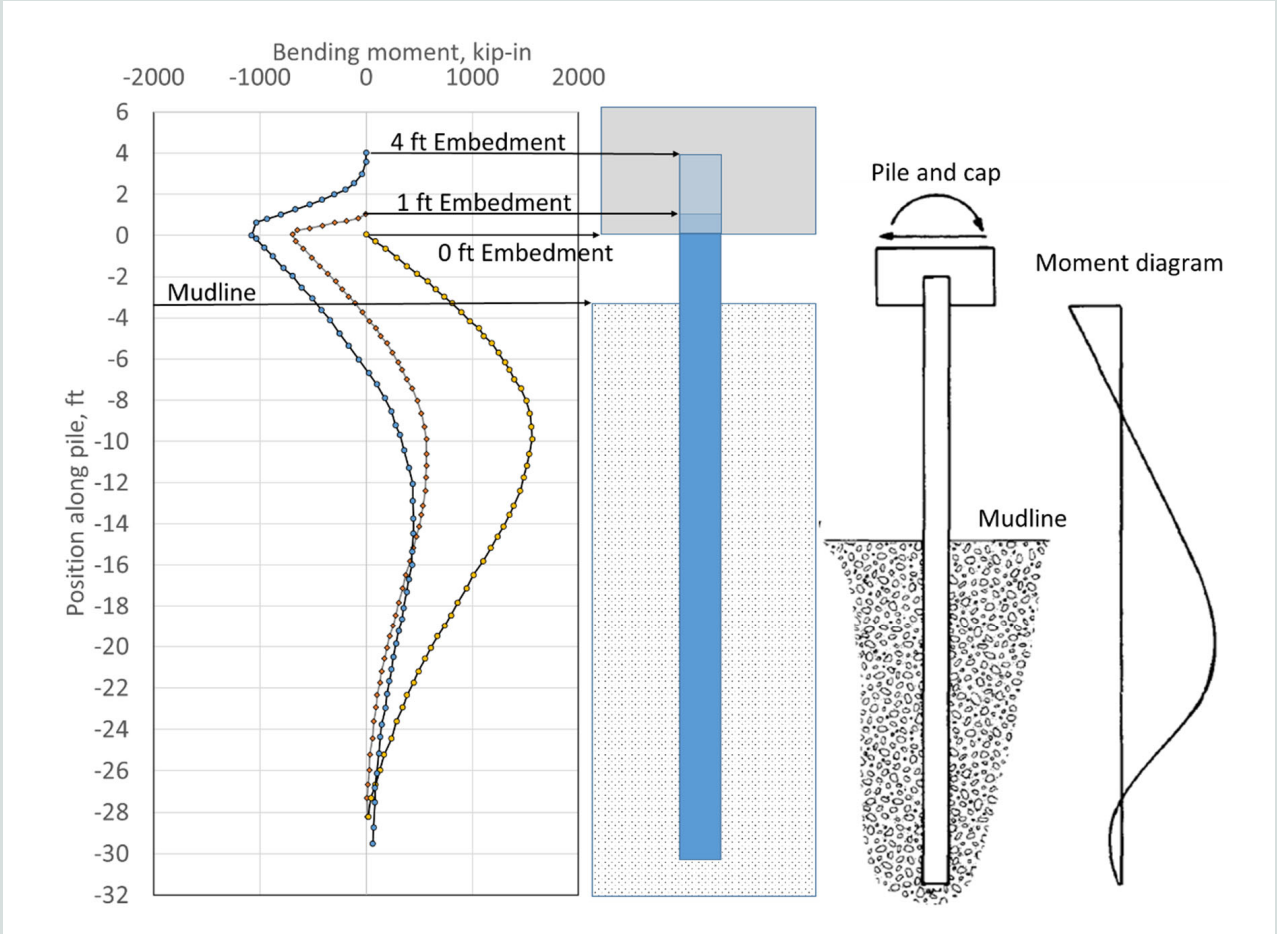

Figure 5. Effect of pile-to-cap fixity/cap embedment depth on moment distribution (left) and misleading moment diagram from Joen and Park (right). Note: 1 ft = 0.305 m; 1 kip-in. = 0.1130 kN. Sources: Digitized from Castilla et al. (1984) (left) and reproduced with permission from Joen and Park (1990) (right).

confusion and has been cited by several subsequent studies where the magnitude of moment was interpreted, and the worst-case moment was stated to exist underground. However, that worst case could only happen when the pile top is not fixed or the cap rotates/distorts significantly.

The FDOT "Structures Design Guidelines" (3.5.1B) designates a 0.3 m (1 ft) minimum embedment, which is considered to constitute a pinned head condition, and Section 3.5.1C considers a 1.2 m (3.9 ft) embedment to be adequate to develop the full bending capacity of pile sizes from 0.3 to 0.76 m (1 to 2.5 ft).[3] However, significant cap-to-pile bond strength (up to 650 psi [4.5 MPa])[13] has been shown to develop around prestressed concrete piles, making the 0.3 m embedment fixed or at least partially fixed, which is supported by Fig. 5 for the steel H-pile. Of the 14 bridges surveyed for this project, all used a 0.3 m embedment, so this criterion was applied to the laboratory test setup for this study.

All the moment diagrams in Fig. 5 correctly indicate a linear change in moment between the cap and the mudline. Below the mudline, the change in moment is directly influenced by the available shear force developed by the lateral soil stiffness. For this study, only the upper portion of the moment diagram was considered important from maximum moment just below the cap to zero moment at the inflection point. This region was shown by the surveys to include the corrosion-damaged region 0.2*L* below the cap. Therefore, a laboratory test setup with an exposed pile length twice the distance from the underside of the cap to the inflection point would accurately reproduce the upper portion of the moment diagram when fixed-end conditions were applied to the top and bottom of piles.

Pier geometry

The pile bent geometry for this study was established based on several factors, including results from damage surveys, the structural response of pile bents under lateral loads, and available facilities for fabricating and testing. Like previous studies, one-third scale model piles were selected to facilitate accurate modeling of the pile geometry and effective prestress.[6] The investigators selected a 152 mm (5.98 in.) square pile that was prestressed by four 7.9 mm ($^5/_{16}$ in.) Grade 1723 MPa (250 ksi) strands jacked to 51.2 kN (11.5 kip) to model the most common 0.46 m (1.5 ft) pile in a pile bent. **Figure 6** shows details of the pile cross section and ties. A range of pile lengths were encountered in the bridges reviewed for this study.[8] Based on that range, as well as the free length of typical prototype piles and the maximum clearance of the laboratory facilities, the model pile length of 3.35 m (11.0 ft) was determined. Likewise, typical bridge bents consisted of four, five, or six piles. Pile cap dimensions and reinforcement details were directly determined from those of the prototype by following modeling principles—that is, by using scale factors n for linear dimensions and n^2 for area values (n for the model was 3). The pile cap width in the prototype bridges was 0.91 m (3.0 ft) while the depth varied between 0.76 m (2.5 ft) and 0.91 m. An exact scale model would be 254 to 305 mm (10.0 to 12.0 in.) deep and 305 mm wide. A model pile cap with a 305 mm square cross section was selected.

To determine the final laboratory-scale model layouts, the investigators used two bridges constructed just before this study, which had five 0.46 m (1.5 ft) piles per bent. The prototype pile bents were analyzed using the in place soil conditions and pile soil embedment with a nonlinear finite element software.

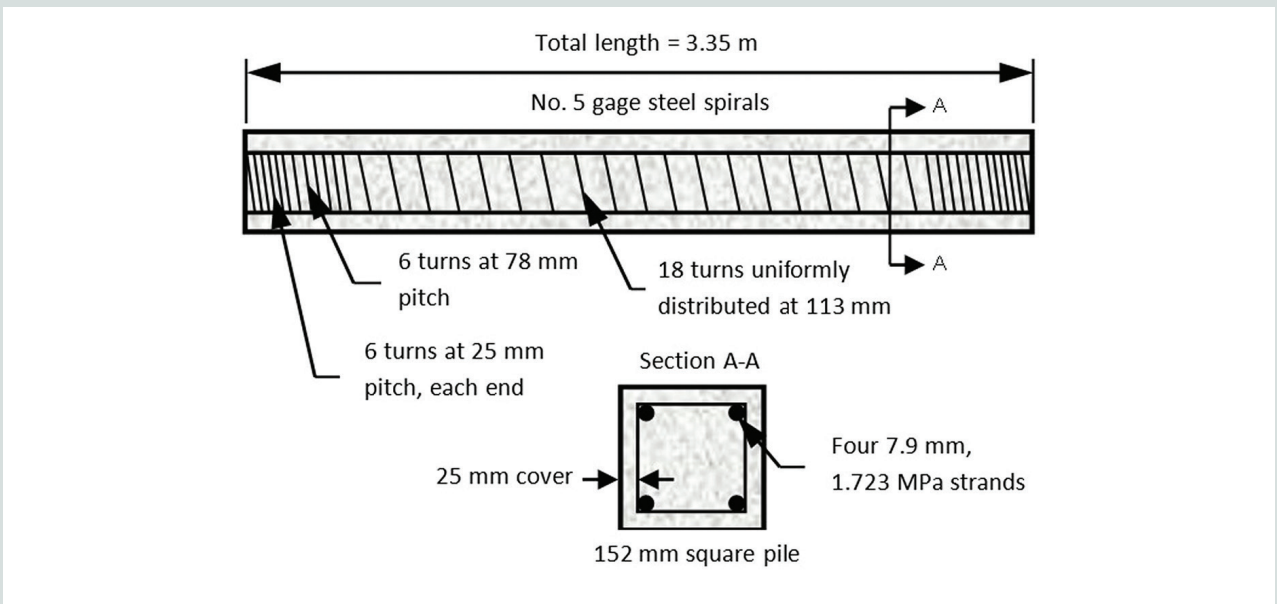

Figure 6. Pile construction details. Note: No. 5 = 16M; 1 mm = 0.0394 in.; 1 m = 3.281 ft; 1 MPa = 0.145 ksi.

The points of inflection for the two bridges occurred 2.9 and 6 m (9.5 and 20 ft) beneath the pile caps, so the corresponding nondimensional ratios were 6.3 and 13.2 pile diameters. As the point of deflection primarily depends on the free length of the pile, a wide range of distances to the inflection point was representative of full-scale conditions for all 74 prototype piers surveyed. Shorter free lengths (in shallow water) translate into lower moments in the damage zone if the damage zone is typically 3 pile diameters beneath the pile cap. In contrast, longer free lengths (in deeper water) place the damage zone farther from the inflection point, in higher moment regions, and are therefore representative of more-severe conditions. The model inflection point was selected to be 10 diameters or 1.52 m (4.99 ft) beneath the pile cap, which corresponded to the maximum pile length that could be tested within the lab. Using a fixed-base condition, the inflection point would occur at the middle of the pile length, so the free length of the model pile would be 3.05 m (10.0 ft). The location of the center of damage was taken as 0.15 of the clear length or 457 mm (18.0 in.) beneath the pile cap. The extent of the damage zone was assumed to be 559 mm (22.0 in.) or one-third of the damaged length of 1.68 m (5.51 ft) chloride contamination region in the prototype bridges noted in previous studies.[14] **Figure 7** shows the bending moment distributions in the two prototype bridge piles along with the finalized model pile layout.

The average slenderness ratio of the piles in the two prototype bridges was 89. Using that ratio and the pile spacing in the field, the pile spacing in the model was determined by equating the stiffness ratios of the prototype and model to be 991 mm (39.0 in.). **Figure 8** shows the finalized dimensions of the model bent. The piles were embedded 102 mm (4.02 in.) into the pile cap, which was one-third of the typical 305 mm (12.0 in.) area in the prototypes. Likewise, cap reinforcement (Grade 410 MPa [60 ksi] steel) for the model pile cap was calculated as one-ninth of the average steel area in the prototypes. The standard Class IV 38 MPa (5500 psi) FDOT concrete design mixture used in the prototype pile caps was also used in the laboratory-scale physical models.

Corrosion simulation

Typically, the type of damage of interest to this study occurs after years of exposure to a combination of moisture, chlorides, and oxygen. These conditions are most prevalent in those regions of the structure that are within the tidal or splash zone, where wetting/splashing and subsequent drying of the concrete surface produces supersaturated salt solutions (in excess of seawater concentrations) in the pores of the con-

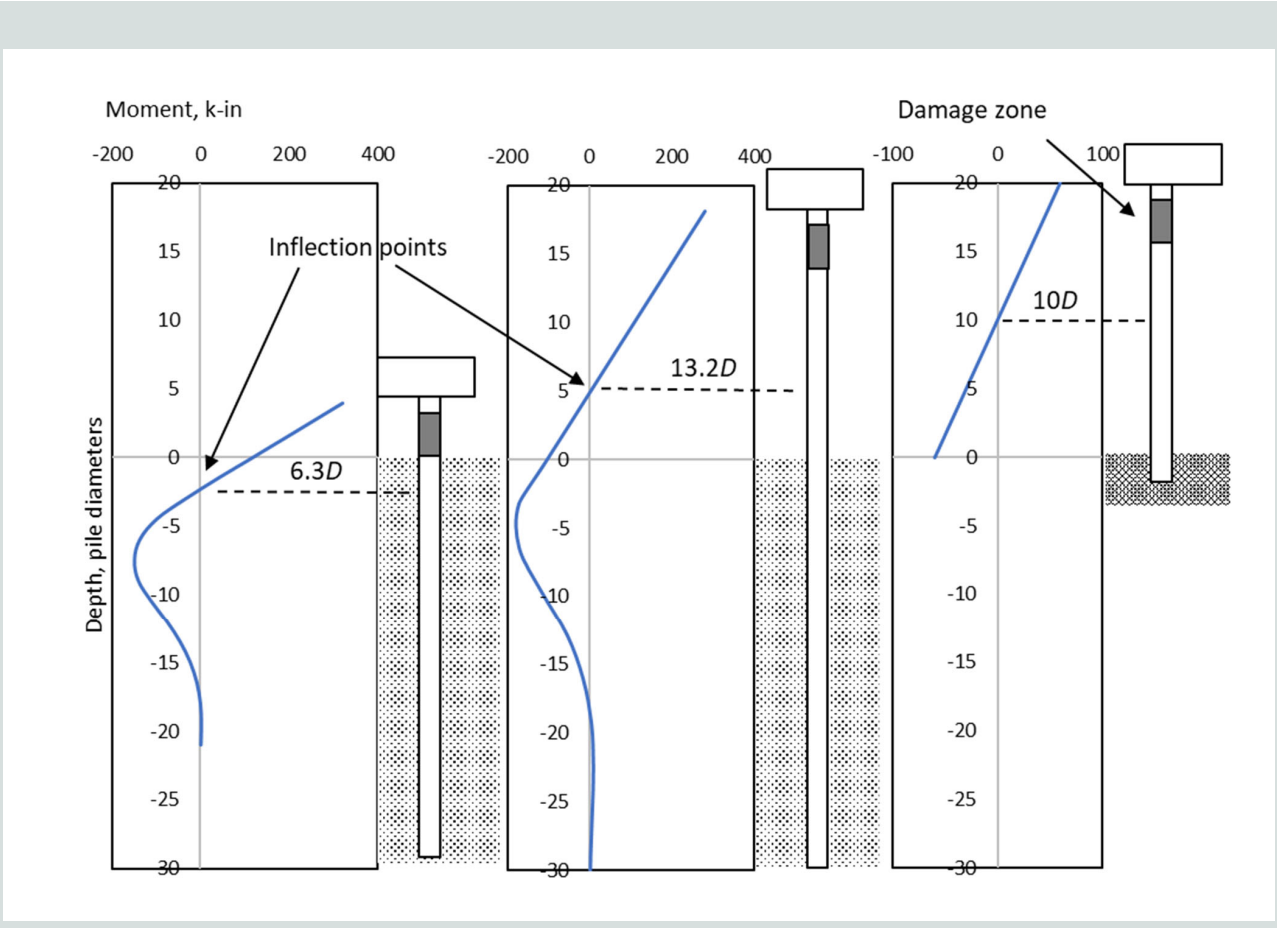

Figure 7. Bending moment distribution in prototype and model piles in a bridge bent. Note: *D* = pile width or diameter. 1 kip-in. = 0.1130 kN.

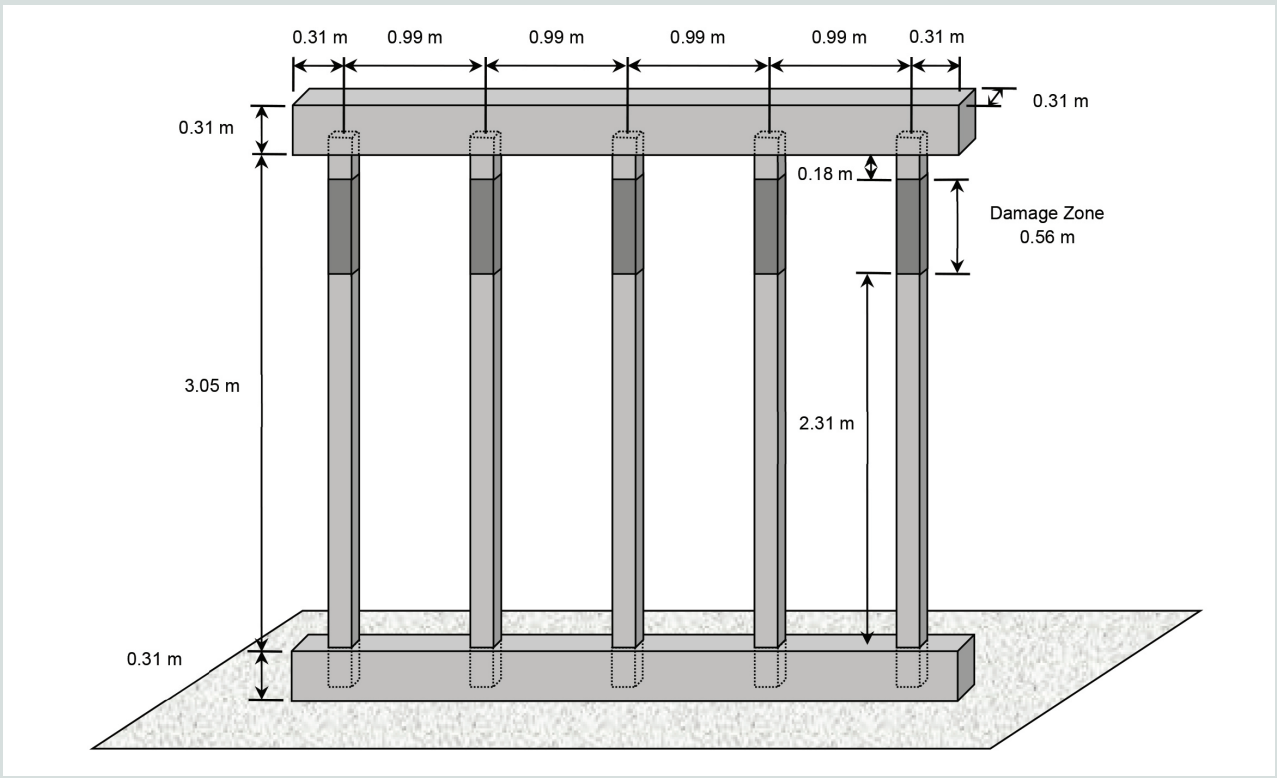

Figure 8. Model pile bent layout. Note: 1 m = 3.281 ft.

crete surface above the seawater level. The increased chloride gradient in these regions of the structure causes exacerbation of the inward diffusion of chlorides. Those regions that are constantly wetted by seawater (below the water surface) never exceed the natural seawater concentrations and therefore have reduced chloride-diffusion rates. Those areas above the splash zone also have lower chloride-diffusion rates; however, in those regions, that is due to the reduced frequency of wetting and lower chloride concentrations on the surface. The parameters required for corrosion—chlorides, oxygen, and moisture—must be integrated into any corrosion-simulation scheme. A convenient method of accelerating corrosion that is widely used by researchers is the impressed current system.[14,15] This type of system can be based on either constant voltage from a direct current (DC) electrical power source or constant current from a DC power source where the positive voltage lead is connected to the reinforcing steel. For this study, the investigators chose a constant-current system because it permits better control of the corrosion rate.

The chloride concentration required to initiate corrosion at the reinforcing steel surface (the critical chloride-concentration threshold) is generally found to be 0.2% to 0.4% of the total cementitious content of the concrete.[16] To eliminate the need for prolonged wet and dry saltwater cycles to introduce chlorides, the prestressed specimens were cast with chloride-contaminated concrete in the regions where corrosion damage was desired. The increased chloride concentration was accomplished by using 53.3 *L*/m^3 (10.8 gal/yd^3) of a water-reducing admixture in the simulated high-chloride-content region of the piles. This additive, which is used as a curing accelerator, contains 279 g/mL (0.0182 lb/fl oz) of chloride ion. The resultant concentration of 3% chlorides by weight of cement exceeded the critical chloride-concentration threshold by tenfold at 15 kg/m^3 (25 lb/yd^3) and therefore would initiate the onset of corrosion. Additionally, 3% chlorides is considered the worst case because higher concentrations can hinder the oxygen dissolution. This chloride concentration was also used in earlier studies.[17]

Both oxygen and moisture should also be present to provide a corrosion cell. Therefore, investigators devised a system to reproduce the in place splash-zone conditions. Therein, the model piles were oriented vertically, and a combination of sponges and soaker hoses was affixed to each specimen to create a corrosion cell. Placing the piles vertically served two purposes: the specimens replicated the natural vertically varying moisture distribution, as opposed to lateral storage, where one face would stay wetter; and the arrangement provided convenient access to each pile and all faces for inspection and servicing. The corrosion cell provided a moist yet not submerged environment through which both oxygen and moisture could be introduced to the simulated damage zone. **Figure 9** shows all piles stored vertically and a close-up view of the corrosion regions equipped with soaker hoses around the piles (top), sponges below a stainless mesh, and the electrical wiring to the mesh on each face of the piles where the negative voltage connection was secured. Rust staining on the

Figure 9. All piles before accelerated corrosion (left) and the simulated splash zone used soaker hoses, sponges, and stainless-steel mesh cathode (right).

Figure 10. Sacrificial pile segments cut open to determine exact steel mass loss.

sponges and piles provides evidence of active corrosion.

The study required multiple specimens to be corroded to specified levels of degradation. The degradation, denoted as the percentage of mass loss of steel, was determined using gravimetric methods that compare the mass of corroded reinforcing steel to the mass of a similar length of uncorroded strand or spiral ties. The gravimetric method entails extracting the steel from the concrete, removing the oxidation, and weighing the remaining steel. However, this procedure is destructive and renders the original specimen unusable for subsequent structural evaluation. For specimens that cannot be destroyed via gravimetric methods, researchers rely on corrosion predictions using Faraday's law. Metal loss estimated using this law assumes 100% efficiency (that is, there are no losses in the transformation of the impressed current to metal loss). Unsurprisingly, predicted losses can overestimate the actual or measured losses. Studies conducted indicated that calculated losses could overestimate actual losses by 150% to 180%.[14] Overestimates as high as 400% were also mentioned in the same reference. A combination of predictive and gravimetric methods were used whereby initial estimates of mass loss were calculated based on constant current and elapsed time. These predictions were then compared to gravimetric results from sacrificial prism specimens not intended for structural testing. The sacrificial prisms, which were shorter-length pile segments (**Fig. 10**) cast alongside the pile specimens in the same prestressing bed, were used only for gravimetric verification. In all, sixty-four 3.4 m (11 ft) long prestressed piles and thirty-two 1 m (3.3 ft) long prism specimens were cast.

A target corrosion current density of 1 μA per mm^2 (0.002 μA per in.^{2}) of steel surface area was selected based on worst-case conditions cited for steel corroding in marine, tropical, or semi-tropical environments.[18] Each pile or prism specimen was connected to a dedicated constant-current circuit where the target (0.002 μA per in.^{2}) current density equated to 120 mA over the 0.56 m (1.8 ft) chloride-contaminated region (**Fig. 11**). Current was gradually increased by 20 mA/day over a 6-day period to minimize but not eliminate localized corrosion (pitting) and provide a more realistic uniform corrosion.[19] Complete details of the constant-current circuit can be found elsewhere.[8,19]

Figure 11. Constant-current control panel showing ammeter and voltmeter monitoring the circuit board output for each specimen.

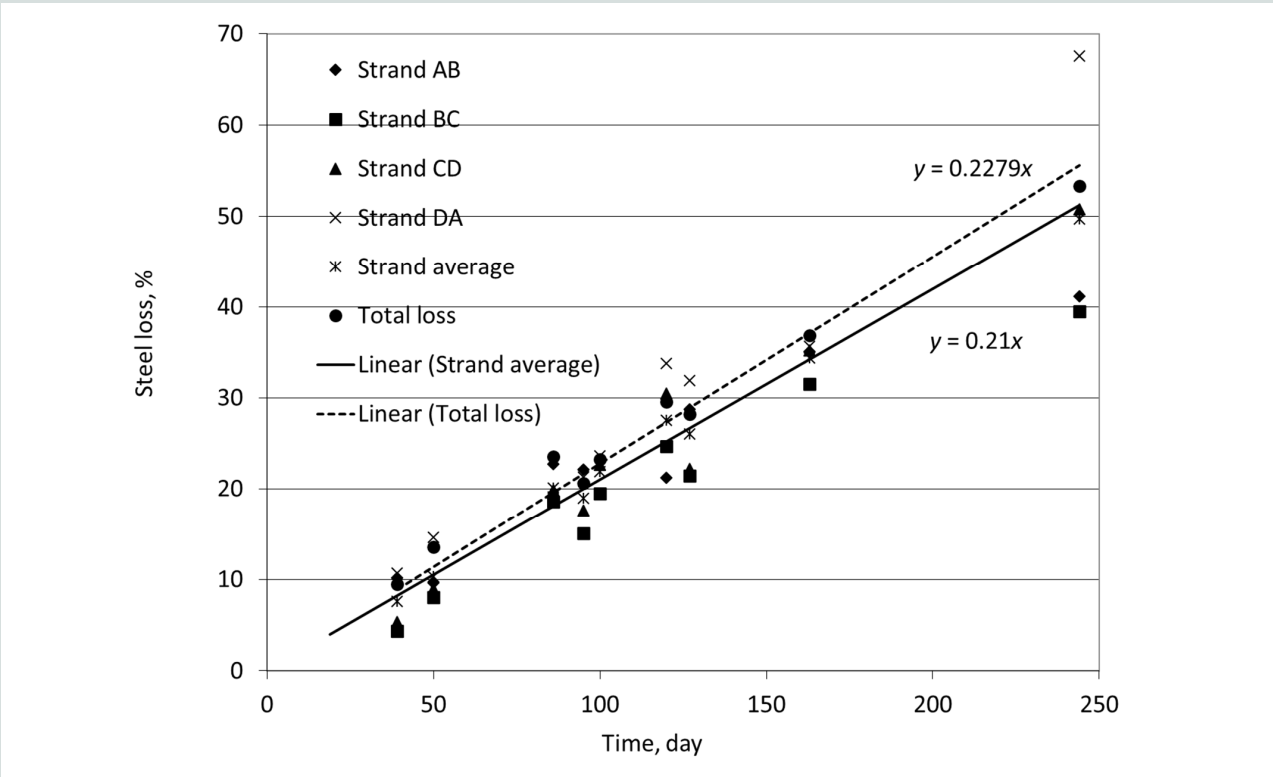

Figure 12. Gravimetric metal loss as a function of time.

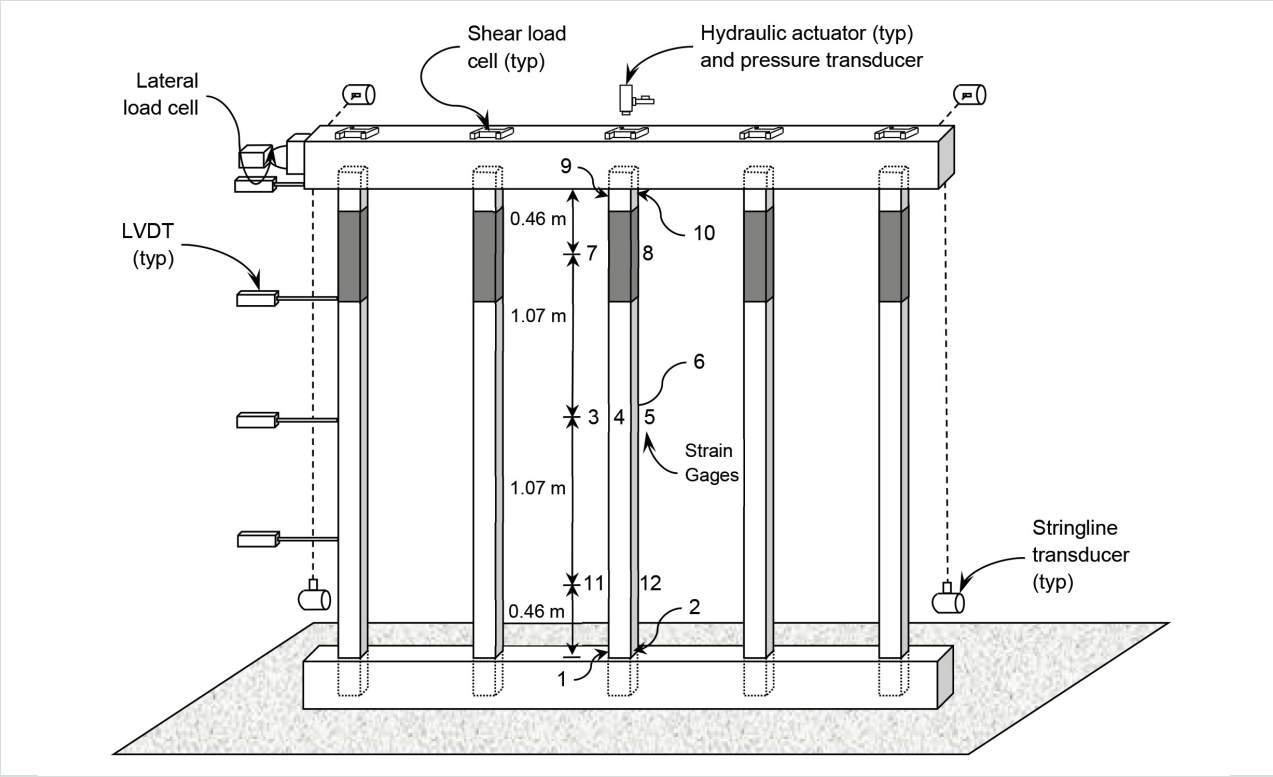

Figure 13. Instrumentation scheme for model pile bents. Note: LVDT = linear variable differential transformer. 1 m = 3.281 ft.

Initial calculations using Faraday's law predicted that 33 days would be required to affect 10% total mass loss of steel. **Figure 12** presents typical results of the gravimetric testing of these prisms. Consistently, the results showed that the stirrups experienced higher percentages of steel loss than the total loss, and the strands just behind the stirrups experienced lower losses. The slopes of the fitted lines indicate 44 days were required to produce 10% total steel mass loss, whereas 48 days were required for a similar degree of corrosion in the primary prestressing strands.

Bridge bent test setup

Five model bridge bents were constructed and tested. The first model was intended to check the test setup system components (axial alignment, displacement, strain gauge placement, data collection system, and feedback controller to axial load actuators); findings from this model are not presented herein. Subsequently, four model bents were tested at prescribed prestressing strand damage levels determined by the percentage of steel mass loss (0%, 10%, 30%, and 50%). The model bents were subjected to axial and lateral loads through hydraulic actuators. An axial load of 44 kN (9.9 kip) was applied to the pile cap above each of the five piles in the model bent to simulate service-level girder loads. A computer-controlled load actuator with a total stroke of 152 mm (5.98 in.) was used to apply the lateral compressive load at one end of the pile cap of the model bent. A trolley system composed of five high-capacity (10 ton [89 kN]) roller assemblies and five axial load actuators was configured to push up against and roll along the underside of the reaction frame girder. Because some of the applied lateral load would be required to push the trolley system, shear cells were introduced between the load actuators and pile cap to differentiate between the load resisted by the piles below the

Table 1. Model pile crack survey

Strand steel loss, %	Average number of cracks per pile	Maximum crack width, mm	Average of maximum crack length, mm
10	6.2	0.5	610
30	7.2	1.5	686
50	10.4	3	775

Note: 1 mm = 0.0394 in.

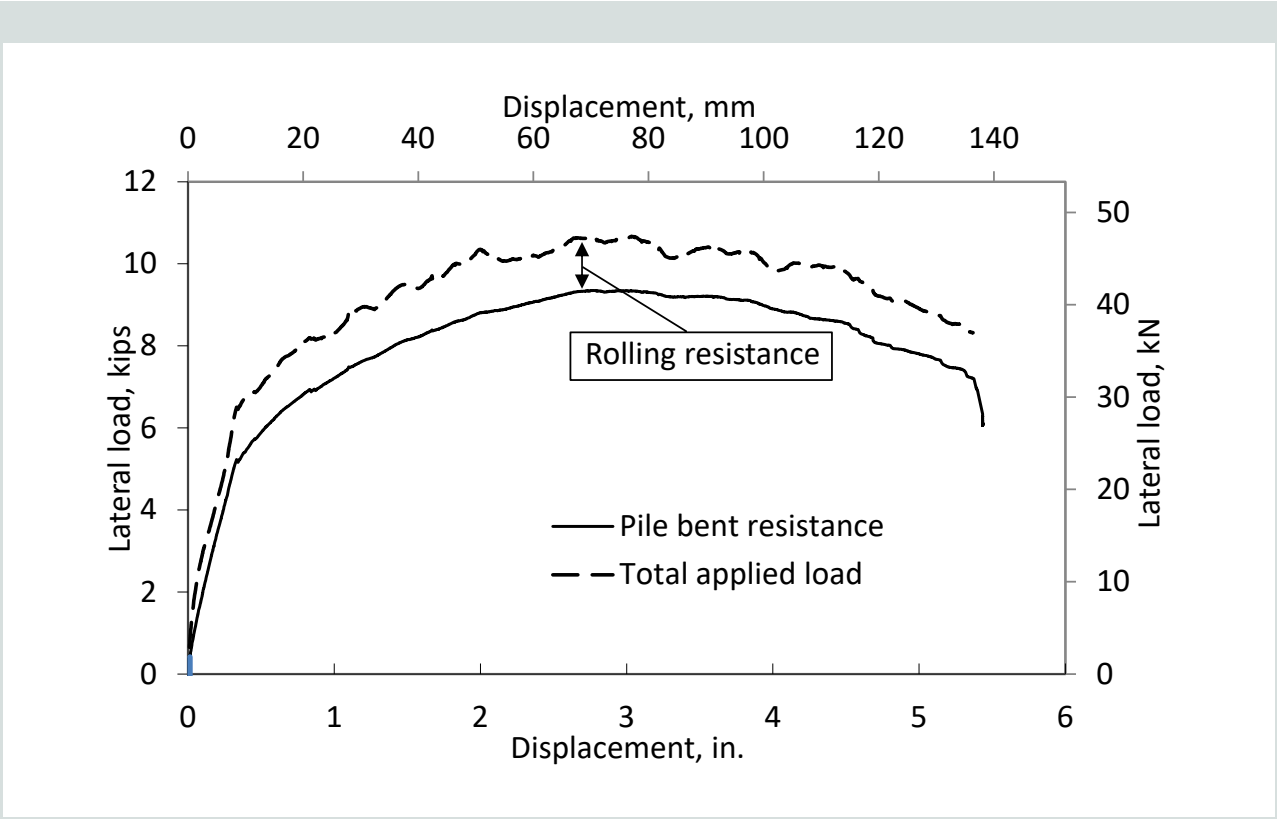

Figure 14. Uncorroded, undamaged control pile bent's load-displacement response corrected for rolling resistance.

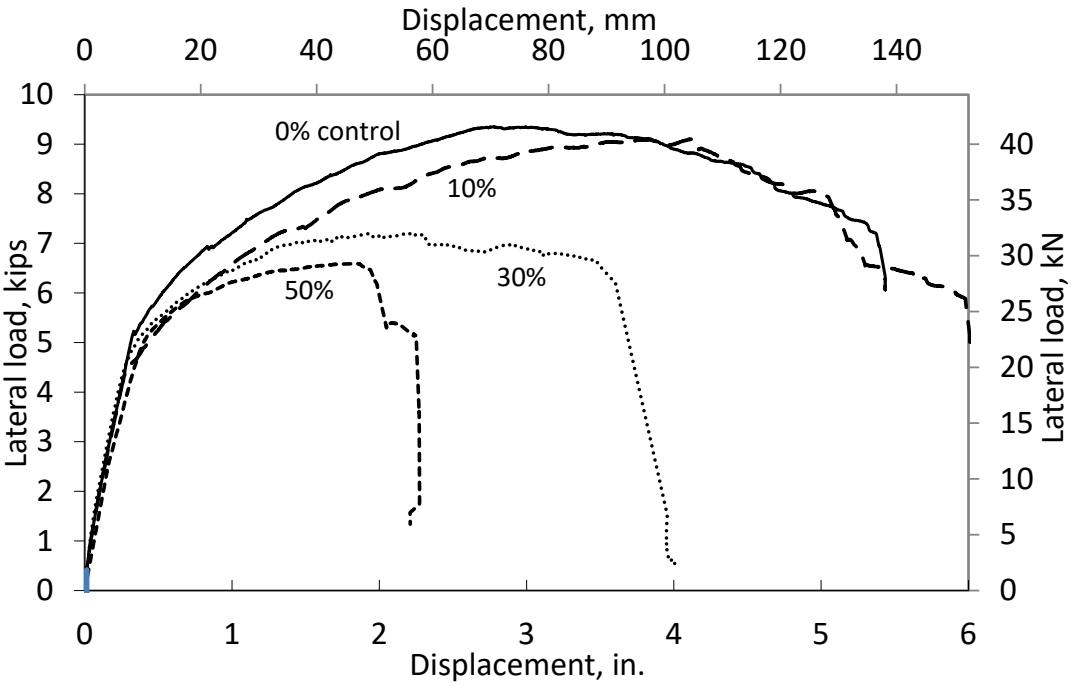

Figure 15. Lateral load versus pile cap displacement for the four pile bents.

Table 2. Summary of lateral-load test results

Model bent, %	Maximum lateral load, kN	Displacement at maximum lateral load, mm	Maximum displacement, mm	Capacity multiplier
0	41.6	70.0	>140	1
10	41.2	106	>152	0.99
30	31.6	57	89	0.76
50	29.3	48	59	0.70

Note: 1 mm = 0.0394 in.; 1 kN = 0.225 kip.

cap and the load required to advance the rolling load actuators above the cap. The lateral loading was applied at a displacement rate of 152 mm (5.98 in.) in 20 minutes. The test was concluded when the lateral-load actuator reached its maximum stroke or the model bent failed catastrophically.

The instrumentation used during each bent test measured applied axial loads, lateral load, rolling resistance of the axial load trolley, in-plane and out-of-plane horizontal displacement, vertical displacement of the pile cap, and strain within the piles. **Figure 13** presents a sketch of the instrumentation setup. Twelve strain gauges were mounted to each pile. The four gauges at the midpoint were used to determine the internal axial load experienced by each of the five piles where bending stresses were expected to be near zero. Gauges were named by pile number-gauge type-gauge number (P1-G060-5 is pile 1, gauge 5) where only 60 mm (2.4 in.) surface-bonded strain gauges were used.

A crack pattern survey was performed on each of the pile specimens after they were cast into the model bents. The sides of each pile were labeled according to their relative position in the casting bed: A was the top face, C was the bottom, and B and D corresponded to the pile sides in the casting bed. **Table 1** summarizes the average number of cracks recorded per pile, the maximum crack width, and the maximum crack length for all piles in each of the three corroded model bents. The crack widths varied with the degree of corrosion and showed significant variations among the faces of each pile. In all corroded specimens, side A (facing up in the cast bed) was found to have the widest cracks. This finding was attributed to

Figure 16. The 50% pile bent before testing.

Figure 17. The 50% bridge bent after catastrophic failure (cap caught by safety chains).

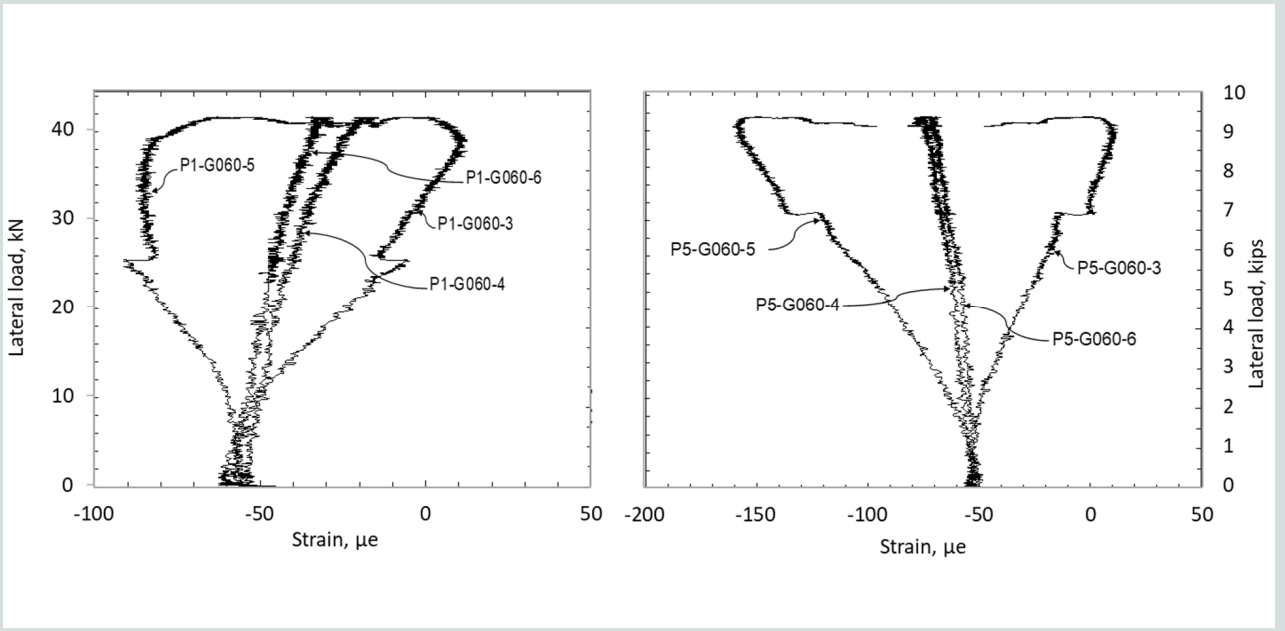

Figure 18. Midheight strains in pile 1 (trailing side) and pile 5 (leading side); 0% steel loss. Note: The gauge nomenclature is pile number-gauge type-gauge number (for example, P1-G060-5 is pile 1 gauge 5).

casting effects, which cause the lower face to be denser than the upper face due to bleed-water effects.

Results

The test setup allowed for vertical service loads to be unchanging and move laterally with the bridge, in a manner similar to a global lateral-loading event such as wind loads. This complexity introduced rolling resistance, which investigators originally expected to be insignificant. However, by separating the total applied lateral load and the load resisted by the piles below, the importance of the shear cell measurements became apparent. **Figure 14** shows the total applied load and the pile bent resistance after the undulat-

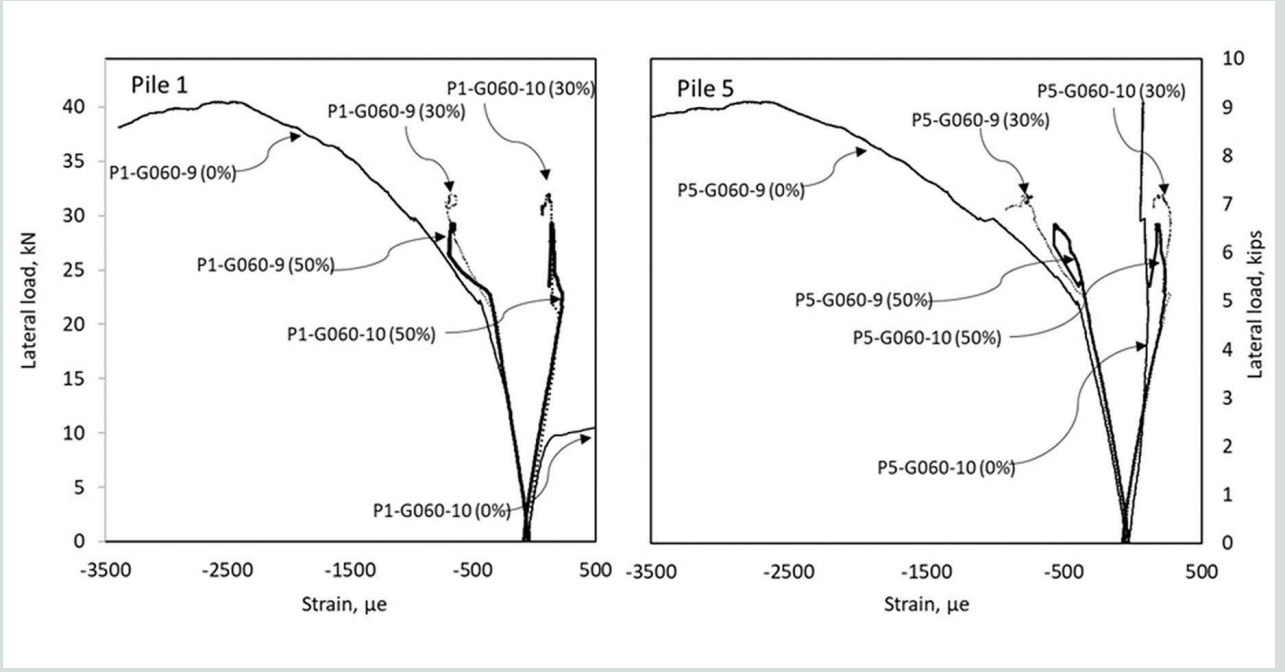

Figure 19. Tension and compression strains in piles 1 and 5 beneath cap.

ing rolling resistance caused by the roller assemblies was subtracted.

Data collected during each of the tests provided the corrected load-displacement response as well as the load-strain response, axial loading, and moments developed in each pile as a function of the lateral load. **Figure 15** shows a graph of the corrected lateral load versus the pile cap displacement for all model bents. **Table 2** summarizes the key data points. The reduction in the lateral capacity due to corrosion damage ranged from 1% for the model bent with 10% steel loss to 30% for the model bent with 50% steel loss. The elastic response of each frame was nearly identical until first cracking. The reduction in stiffness after first cracking corresponded to the reduction in ultimate capacity of the various model bents. The failure modes consisted of cracking and spalling, mainly in the upper and lower ends of the piles. Cracking and spalling were more widespread with higher levels of corrosion damage, which included the amount of concrete cover in the damage zones that fully delaminated. In the 30% model bent, three of the five piles failed catastrophically in the damage zone. All five piles failed catastrophically in the damage zone of the 50% model bent. The top portion of the piles with 50% steel loss during the test developed a hinge in the piles, indicating a shear-type failure mode rather than classic frame-bending behavior. **Figures 16** and **17** show the 50% model bent before and immediately after testing, respectively.

Discussion

The reductions in load resistance and ductility were shown to be proportional to the steel-strand section loss. For the control pile bent, bending moments were nearly identical at the cap with a 102 mm (4.02 in.) embedment and at the fixed connection formed with the laboratory floor, where a 203 mm (7.99 in.) embedment was provided. This finding indicates that the 102 mm embedment provided a fixed or nearly fixed head condition. Under these conditions, a prediction of the axial-loading behavior of each pile as the lateral load is applied can be made using the portal method.[20] Therein, the axial load for the leading pile in the group (away from the applied lateral load) should increase while axial load for the trailing pile should decrease. This trend (**Fig. 18**) was consistent throughout the control test where the average compression strain in piles 1 and 5 decreased and increased, respectively. However, after initial cracking, the inflection point began to move up the pile, indicating a loss of fixity near the cap or a reduction in pile stiffness in the damage zone. This is evidenced by an increase in tensile strains in gauge 3 or compression strains in gauge 5 located at midheight on the trailing and leading sides of the piles, respectively. Pile 1 (Fig. 18) cracked first at 25.8 kN (5.80 kip) and pile 5 cracked last at 39.4 kN (8.86 kip) due to the decrease and increase in their axial loads, respectively, from portal frame action.

Loss of fixity in a prestressed concrete pile can be the result of the pile-to-pile cap bond being broken, concrete crushing (cap or pile), or strand slippage/inability to develop the strand. The latter is the most likely explanation of loss of fixity for this case. The 102 mm (4.02 in.) embedment equates to approximately 13 diameters of the 7.9 mm (5⁄16 in.) model strands, which is not sufficient for development. The prototype piles with 0.3 m (1 ft) embedment and 12.7 mm (0.500 in.) strands provide approximately 24 diameters of the strand for develop-

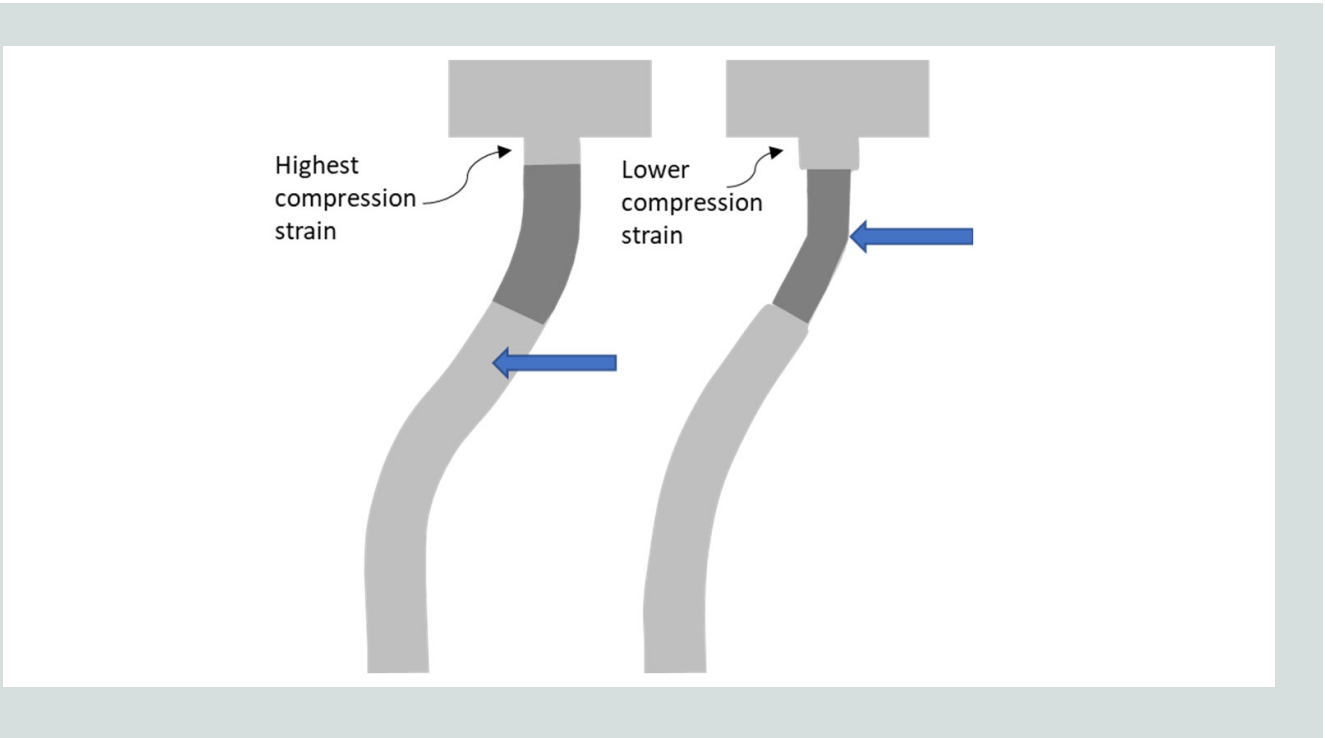

Figure 20. Inflection point transition from midheight to location of hinge.

ment just below the pile cap, which likely improves performance. Nevertheless, the model piles exhibited high bending moments at the cap. Investigators could not use the 30% and 50% pile bents to test the pile-to-pile cap fixity because pile failures occurred in lower bending moment regions where corrosion damage severely compromised the section. **Figure 19** shows the top of pile strains approximately 50 mm (2.0 in.) below the cap again for piles 1 and 5 for the 0%, 30%, and 50% pile bents. The 10% response was similar to the 0% bent and is not shown to minimize clutter.

Whereas gauges 4 and 6 in Fig. 18 were largely dominated by the increase or decrease in axial force caused by portal frame action, gauges 3 and 5 show the superposition of axial and bending stresses where strain is determined by $P/AE \pm My/IE$ where P is the axial load, A is the cross sectional area, E is the composite modulus, M is the bending moment; y is the distance from the neutral axis; I is the moment of inertia, P/A represents axial stress, and My/I is the bending stress. Similar to gauges 3 and 5 in Fig. 18, the strains in Fig. 19 show only the combined effects at the extreme edges; however, Fig. 19 shows the effects in the highest bending moment portion of the piles just beneath the cap. In all tests, the difference in compression and tension strains at a given load is an indication of bending moment magnitude. When looking only at gauge 9 (compression side, below the cap), the individual pile bent responses were similar up to approximately 22 kN (4.9 kip) (Fig. 15). For the control bent (0% steel loss), the rapid strain increase in gauge 10 on pile 1 indicates that a crack formed within the length of the 60 mm (2.4 in.) gauge length; results for pile 5 were nearly identical, except that the crack formed adjacent to gauge 10, so no additional strain was transferred into the surface concrete under the gauge after cracking. In the 30% and 50% pile bents, no cracking occurred under or near gauge 10. Rather, pile failure occurred in the lower-moment regions coinciding with the steel-loss locations.

The compressive strains at the gauge 9 location in all piles indicate that the bending moment magnitude M (equal to $IE\epsilon/y$, where ϵ is strain) in the 30% and 50% bents were unable to develop an appreciable increase in bending moment after first cracking due to failures in the damage zone. The mode of failures began with concrete crushing and spalling cover loss, followed by complete loss in bending resistance in the damage zone resulting in a hinge in the approximate center of damage zone. This mode of failure caused a reduction in compressive strains (gauge 9) as the rigid pile cap connection now resisted only a simple cantilevered bending moment with a shorter moment arm. **Figure 20** shows the conceptual transition from fully fixed portal frame conditions, where the zero-moment inflection point at midheight in the pile moved up to the location of a zero-moment hinge in the damaged region. The translation in the inflection point reduced the moment arm from $0.5L$ to $0.15L$, where the system shear force can be used to directly compute the maximum pile bending moment beneath the cap. The translation was accompanied by a reduction in the resisting force offered by the pile bent. The 0% control and 10% pile bents showed that the top of all piles failed in concrete crushing at compression strains greater than 3000 μe. This finding indicates that even if fixity were not completely maintained with no rotation, the connection was sufficient to fully develop the pile bending capacity.

Conclusion

The corrosion damage imposed on the model piles was similar to that observed in prototype piles. Longitudinal cracking, partial delamination of cover, and zones of complete loss of strand cross section were observed. The pile damage due to the corrosion of the prestressing strands was documented by crack surveys, gravimetric testing, and photographs. The constant-current accelerated corrosion system was also shown to be effective. Targeted corrosion loss levels (verified by actual loss measurements through gravimetric testing) were predictable and obtained within a relatively short time frame. An average of 10% prestressing strand steel mass loss was achieved every 48 days at the 1 µA per mm² (0.002 µA per in.^{2}) impressed current.

The prime objective of the study was to assess the effect of corrosion damage on lateral capacity reduction in pile bents while under axial service loads. The test results indicated that while ultimate capacity decreased, stiffness response to moderate or everyday lateral loads was relatively unchanged. However, there was considerable reduction in ductility in specimens corroded to 30% and 50% just after linearity that led to sudden and catastrophic failure. Brief details are as follows:

- 10% model bent: The reduction of the ultimate lateral capacity of this bent was minimal at approximately 1% reduction. The load-displacement response demonstrated a softer response after yielding but withstood large deformations up to 152 mm (5.98 in.) without collapse.

- 30% model bent: The reduction of the ultimate lateral capacity was more severe at this level of damage, proving to be 24% less than the uncorroded control. Although the initial stiffness of the load-displacement response was similar to the control, the cracking load was slightly reduced by 1.8 kN (0.40 kip), and ultimate capacity was achieved at a displacement 13 mm (0.51 in.) less. Catastrophic failure in three out of the five piles occurred at a displacement of 89 mm (3.5 in.).

- 50% model bent: The reduction of the ultimate lateral capacity was 30%. The stiffness of the pile bent was initially slightly less than the control, and its ultimate capacity occurred at a displacement that was 25 mm (0.98 in.) less than the control. Catastrophic failure occurred in all five piles at a displacement of 59 mm (2.3 in.), less than half the ductility demonstrated by the control and 10% pile bents.

Although the test results do not suggest alarming implications for everyday loads on bridges that exhibit corrosion

damage, the location of damage relative to high bending-moment regions must be considered when assessing the severity of a given bridge condition. In such an assessment, it should be assumed that "pinned" end conditions at the pile cap are more likely to respond as a fixed end, and whichever case (fixed or pinned) gives a higher moment at the location of damage should therefore be assumed. Finally, designs for extreme events such as vessel collisions require that the structure can survive and be repairable. A bridge with 30% steel loss or greater (demonstrated by delamination and cover loss) is unlikely to demonstrate the ductility required.

Acknowledgments

This study was originally funded by a grant from the Florida Department of Transportation. The opinions, findings, and conclusions expressed in this publication are those of the authors and not necessarily those of the Florida Department of Transportation or the U.S. Department of Transportation. The authors would also like to thank Dr. Kwangsuk Suh for his contributions.

References

1. Al Azzawi, M., P. Hopkins, G. Mullins, and R. Sen. 2018. "FRP–Concrete Bond after 12-Year Exposure in Tidal Waters." *ASCE Journal of Composites for Construction* 22 (5). https://doi.org/10.1061/(ASCE)CC.1943-5614.0000864.

2. Robertson, D., M. Muchard, G. Mullins, and D. Brown. 2000. "Lateral Statnamic Load Testing: A New Method for Evaluating Lateral Load Capacity." In *Statnamic Loading Test: Proceedings of the 2nd International Statnamic Seminar, Tokyo, Japan, 28–30 October 1998*, edited by O. Kusokabe, F. Kuabara, and T. Matsumoto. Boca Raton, FL: CRC Press.

3. FDOT (Florida Department of Transportation) Structures Design Office. 2022. "Structures Design Guidelines." In *FDOT Structures Design Manual*. Tallahassee, FL: FDOT.

4. AASHTO (Association of State Highway and Transportation Officials). 2022. *AASHTO LRFD Bridge Design Specifications*. 9th ed. Washington, DC: AASHTO.

5. Clark, J. D. 2019. *Florida Department of Transportation Bridge Inventory 2019 Annual Report*. Tallahassee, FL: FDOT. https://www.fdot.gov/maintenance/bridgeinfo.shtm.

6. Sen, R., G. Mullins, and D. Snyder. 1999. *Ultimate Capacity of Corrosion Damaged Piles*. Final report. Tallahassee, FL: FDOT.

7. Hartt, W., and M. Rapa. 1998. *Condition Assessment of Jackets upon Pilings for Florida Bridge Substructures—Task II and III*. Final report. Tallahassee, FL: FDOT.

8. Mullins, G., and R. Sen. 2001. *Lateral Capacity of Corroded Pile Bents*. Final report. Tallahassee, FL: FDOT.

9. Sen, R., G. Mullins, K. S. Suh, and D. Winters. 2005. "FRP Application in Underwater Repair of Corroded Piles." *ACI Special Publications* 230: 1139–1156. https://doi.org/10.14359/14885.

10. Mullins, G., R. Sen, K. Suh, and D. Winters. 2005. "Underwater Fiber-Reinforced Polymers Repair of Prestressed Piles in the Allen Creek Bridge." *Journal of Composites for Construction* 9 (2): 136–146. https://doi.org/10.1061/(ASCE)1090-0268(2005)9:2(136).

11. Castilla, F., P. Martin, and J. Link. 1984. *Fixity of Members Embedded in Concrete*. Champaign, IL: US Army Corps of Engineers. https://apps.dtic.mil/sti/tr/pdf/ADA138862.pdf.

12. Joen, P., and R. Park. 1990. "Simulated Seismic Load Tests on Prestressed Concrete Piles and Pile-Pile Cap Connections." *PCI Journal* 35 (6): 42–61. https://doi.org/10.15554/pcij.11011990.42.61.

13. Mullins, G., R. Sosa, R. Sen, and M. Issa. 2001. "Seal Slab Prestressed Pile Interface Bond from Full-Scale Testing." *ACI Structural Journal* 98 (5): 743–751. https://doi.org/10.14359/10628.

14. Mangat, P. S., and M. S. Elgarf. 1999. "Flexural Strength of Concrete Beams with Corroding Reinforcement." *ACI Structural Journal* 96. (1): 149–158. https://doi.org/10.14359/606.

15. Lee, C., J. Bonacci, M. Thomas, M. Maalej, S. Khajehour, N. Hearn, S. Panatazopoulo, and S. Sheikh. 2000. "Accelerated Corrosion and Repair of Reinforced Concrete Columns Using Carbon Fiber Reinforced Polymer Sheets." *Canadian Journal of Civil Engineering* 27 (5): 941–948. https://doi.org/10.1139/l00-030.

16. Sagüés, A. A., and S. C. Kranc. 2001. *Corrosion Forecasting for 75-Year Durability Design of Reinforced Concrete*. Final Report. Tallahassee, FL: FDOT. https://fdotwww.blob.core.windows.net/sitefinity/docs/default-source/research/reports/fdot-805-rev-4-17-06.pdf.

17. Torres-Acosta, A. A., and A. A. Sagüés. 2000. "Concrete Cover Cracking with Localized Corrosion of Reinforcing Steel." *ACI Symposium Papers* 192: 591–611. https://doi.org/10.14359/5773.

18. Jones, D. A. 1996. *Principles and Prevention of Corrosion*. 2nd ed. Upper Saddle River, NJ: Prentice-Hall.

19. Goulish, A. 2001. "Lateral Capacity of Corrosion

Damaged Pile Bents." master's thesis, University of South Florida, Department of Civil and Environmental Engineering.

20. Sack, R. L. 1984. *Structural Analysis*. New York, NY: McGraw-Hill.

Notation

A = cross sectional area of the pile

D = pile width or diameter

E = composite modulus

I = moment of inertia

L = length of pile from the underside of the cap to the point of fixity below ground

M = bending moment

n = scale factor

P = axial load

r = radius of gyration

y = distance from neutral axis

About the authors

Gray Mullins is a professor in the Department of Civil and Environmental Engineering at the University of South Florida in Tampa, Fla.

Rajan Sen is professor emeritus in the Department of Civil and Environmental Engineering at the University of South Florida.

Andrew Goulish is executive vice president for Ryan Hughes Design in Tampa.

Danny Winters is senior geotechnical engineer at Foundation & Geotechnical Engineering LLC in Plant City, Fla.

Abstract

The effects of corrosion damage in prestressed piles are difficult to quantify because the amounts of steel loss are unknown. An experimental study was conducted to investigate the lateral capacity of corroded pile bents compared with that of an identical uncorroded pile bent. Based on field surveys of damaged pile bents, investigators constructed five-pile bent specimens (one-third scale) and laterally loaded them to failure. Corrosion damage in the model piles represented steel losses of 10%, 30%, and 50%. The three corroded pile bents experienced 1%, 24%, and 30% ultimate capacity reduction, respectively. Ductility was more affected at high levels of corrosion, where the failure displacement was reduced by 42% and 62% for the 30% and 50% pile bents, respectively. Both the control pile bent and the pile bent with 10% steel loss withstood the full lateral movement of the tests, whereas the specimens with 30% and 50% steel losses experienced catastrophic failures. This paper, which is the first in a three-part series highlighting the test methodologies and effects of corrosion damage on bridge pile bents, provides the basis of comparison for two subsequent papers. Part 2 will address the design of carbon-fiber-reinforced polymer (CFRP) repairs for corroded piles, and part 3 will present test results for a severely corroded pile bent where full lateral capacity was restored using CFRP repairs.

Keywords

Bridge piers, corrosion damage, lateral capacity, pile bent, steel loss.

Review policy

This paper was reviewed in accordance with the Precast/Prestressed Concrete Institute's peer-review process. The Precast/Prestressed Concrete Institute is not responsible for statements made by authors of papers in *PCI Journal*. No payment is offered.

Publishing details

This paper appears in *PCI Journal* (ISSN 0887-9672) V. 70, No. 2, March–April 2025, and can be found at https://doi.org./10.15554/pcij70.2-02. *PCI Journal* is published bimonthly by the Precast/Prestressed Concrete Institute, 8770 W. Bryn Mawr Ave., Suite 1150, Chicago, IL 60631.

Reader comments

Please address any reader comments to *PCI Journal* editor-in-chief Tom Klemens at tklemens@pci.org or Precast/Prestressed Concrete Institute, c/o *PCI Journal*, 8770 W. Bryn Mawr Ave., Suite 1150, Chicago, IL 60631.